Removal of Levofloxacin Antibiotic in Water by Photocatalysis using TiO_2-Based Materials

Tran Quoc Thao[1,2], Pham Tan Thi[1,3], Pham Tran Ngoc Tu[1,2], Nguyen Thi Thuy[2,4], Nguyen Lan Thanh[1,2], Nguyen Thi Hoang Hai[2,4], Nguyen Hai Au[2,5], Nguyen Thanh Hai[2,6] and Nguyen Nhat Huy[1,2]*

[1]Faculty of Environment and Natural Resources, Ho Chi Minh City University of Technology (HCMUT), 268 Ly Thuong Kiet St., Dist. 10, Ho Chi Minh City, Vietnam

[2]Vietnam National University Ho Chi Minh City, Linh Trung Ward, Thu Duc City, Ho Chi Minh City, Vietnam

[3]Faculty of Applied Science, Ho Chi Minh City University of Technology (HCMUT), 268 Ly Thuong Kiet St., Dist. 10, Ho Chi Minh City, Vietnam

[4]School of Chemical and Environmental Engineering, International University, Quarter 6, Linh Trung Ward, Thu Duc District, Ho Chi Minh City, Vietnam

[5]Department of Remote Sensing and Geospatial Information System, Institute for Environment and Resources, 142 To Hien Thanh St., Dist. 10, Ho Chi Minh City, Vietnam

[6]Faculty of Geography, University of Social Sciences and Humanities, 10-12 Dinh Tien Hoang St., Ben Nghe Ward, District 1, Ho Chi Minh City, Vietnam

*Corresponding author (e-mail: nnhuy@hcmut.edu.vn)

This study investigated TiO_2-based photocatalysts for degrading levofloxacin (LEVO), addressing the environmental and health risks posed by antibiotic residues in water. Various TiO_2-based materials were examined: commercial TiO_2 (P25, Degussa, Germany), TiO_2/ZnO (hydrothermal synthesis), as well as Pd-, Pt-, and Ag-doped TiO_2 (sol-gel synthesis). Optimal conditions included pH 4, a 1:20 LEVO-to-photocatalyst ratio, and 150 minutes. P25 achieved the highest efficiency (85 %) within 180 minutes, outperforming synthesized catalysts at shorter durations. Sol-gel-derived catalysts demonstrated better performance for extended reaction times, achieving 69.36 % efficiency after 150 minutes, while TiO_2/ZnO reached 14.03 %. Treatment efficiency decreased at higher pH levels, dropping to 2.81 % at pH 9. The Langmuir-Hinshelwood model (R^2 = 0.9862) described the reaction mechanism effectively. This study highlights TiO_2-based photocatalysis as a viable solution for antibiotic removal, with P25 identified as the most effective catalyst for shorter reactions while sol-gel catalysts excelled at longer durations.

Keywords: Levofloxacin; photocatalysis; TiO_2 nanomaterial; antibiotic residues; water treatment

Received: October 2024; Accepted: March 2025

The challenge of providing effective initial antibiotic treatment is escalating due to antibiotic-resistant bacteria, leading to higher mortality rates, prolonged hospitalizations, and elevated treatment costs [1]. In Vietnam, the medical industry faces significant challenges related to the high prevalence of antibiotic-resistant pathogens, particularly in hospital-acquired infections such as ventilator-associated pneumonia caused by antibiotic-resistant Gram-negative pathogens like *Acinetobacter baumannii* and *Pseudomonas aeruginosa*. *Acinetobacter baumannii* shows up to 99 % resistance to group 2 carbapenems and levofloxacin, while *Pseudomonas aeruginosa* demonstrates resistance rates exceeding 70 %, with levofloxacin being the most resistant among fluoroquinolones [2]. Additionally, Gram-negative bacteria like *Escherichia coli* and *Staphylococcus aureus* display alarming resistance levels, emphasising the urgency of addressing antibiotic resistance in healthcare [3]. These trends exacerbate the burden on Vietnam's healthcare system, leading to poorer patient outcomes, increased economic strain, and a higher risk of treatment failures.

Globally, antibiotic residues in aquatic environments present a critical environmental and public health challenge. Wastewater from pharmaceutical industries, hospitals, and agricultural runoff has been identified as a major contributor to the widespread presence of antibiotics in surface water, groundwater, and even drinking water supplies [4]. These residues not only exacerbate the development of antibiotic resistance genes (ARGs) in microbial communities but also pose ecotoxicological risks to aquatic ecosystems and human health [5]. The persistence of fluoroquinolone antibiotics like *levofloxacin* (LEVO) in water systems underscores the global urgency to develop efficient and environmentally sustainable removal technologies.

Given the growing environmental risks posed by antibiotic residues, it is crucial to explore and

develop effective methods for their removal from water systems. LEVO, a powerful asymmetric fluorinated carboxyquinolone, is effective against Gram-negative and Gram-positive bacteria, making it valuable for treating sinusitis, urinary tract infections, and community-acquired pneumonia [6]. LEVO has been detected in various aquatic environments, with concentrations ranging from 213 µg/L in river water to 170–2,168 ng/L in wastewater treatment plant effluents [7]. In industrial wastewater, concentrations can vary from 0.91 ng/L to 99.3 ng/L, and up to 19,981 ng/L in extreme cases [8]. Such high concentrations, particularly in developing countries with inadequate industrial wastewater treatment, highlight the urgent need for effective degradation methods to mitigate environmental and health risks.

Researchers are exploring methods to address antibiotic residues, with conventional approaches often falling short due to biodegradation challenges [9]. Biological methods relying on bacteria and microorganisms lead to resistance genes, underscoring the need for innovative treatments. Advanced oxidation processes (AOPs) have gained prominence, utilizing highly reactive radicals like the hydroxyl radical ($HO^{\bullet}$) to enhance treatment methods [10]. Photocatalysis, employing catalysts such as TiO_2, ZnO, ZnS, Fe_2O_3, CdS, and WO_3, is a promising approach for mineralizing challenging organic compounds [11]. While the Fenton process is effective in removing LEVO, it generates environmentally problematic iron sludge [12]. In Vietnam, studies are focussed on addressing fluoroquinolone residues in hospital wastewater [13].

Titanium dioxide (TiO_2) shows significant potential in removing antibiotic residues from diverse sources [14, 15]. With excellent photocatalytic properties, TiO_2 breaks down antibiotic residues into harmless byproducts, presenting an environmentally friendly solution [16]. This study evaluates LEVO removal through photocatalysis, utilizing different modified catalysts, predominantly TiO_2. The sol-gel and hydrothermal methods were selected for synthesizing TiO_2-based photocatalysts due to their ability to produce high surface-area materials with well-controlled morphology and structure, critical for enhancing photocatalytic performance. The sol-gel method is particularly known for producing uniform, highly porous materials, which improve the dispersion of the catalyst and promote better interaction with pollutants [17]. Meanwhile, the hydrothermal method allows for the synthesis of TiO_2 with a more crystalline structure, which has been shown to improve its stability and photocatalytic efficiency under UV light [18].

Zinc oxide (ZnO) is another widely studied photocatalyst due to its low cost, high catalytic activity, and ability to degrade a wide range of pollutants under UV light [19]. ZnO nanoparticles have been reported to have significant potential for degrading antibiotic residues, and their performance can be influenced by factors such as particle size, surface area, and the presence of defects or doping agents [20]. ZnO's photocatalytic activity is comparable to that of TiO_2 in many applications; it has also shown promise in eliminating organic contaminants in water, including antibiotic compounds like LEVO.

Graphene oxide (GO) is another promising material for photocatalysis due to its unique properties, including a large surface area, high conductivity, and strong adsorption ability, which facilitate the efficient removal of pollutants [21]. GO can be combined with TiO_2 or ZnO to form composite photocatalysts that enhance the overall photocatalytic activity by improving electron transfer, reducing recombination rates, and increasing the catalyst's stability [22, 23]. The incorporation of GO into photocatalysts has shown to increase the photocatalytic degradation of antibiotics, including LEVO, by improving the catalyst's performance in terms of both efficiency and stability.

This study aims to contribute to the development of more efficient and sustainable photocatalytic water treatment solutions for removing antibiotic residues, addressing an urgent environmental and public health issue. We examined various TiO_2-based photocatalysts, including commercial P25 Degussa and those synthesized via sol-gel and hydrothermal methods, for their potential in degrading LEVO. By investigating how synthesis methods influence photocatalytic efficiency and exploring key reaction parameters such as pH, antibiotic-to-catalyst ratio, and reaction time, this study enhances the understanding of photocatalysis for removing antibiotic pollutants. Furthermore, the application of a kinetic model to optimize the photocatalytic ratio offers a deeper insight into pollutant concentration and treatment efficiency, improving the potential for scalable, environmentally friendly water treatment systems.

MATERIALS AND METHODS

Chemicals and Characterization

LEVO (99 % purity, Henan, China), with the chemical formula $C_{10}H_{20}FN_3O_4$, a molecular weight of 361.4 g/mol, and CAS Number 100986-85-4, was used as the antibiotic. TiO_2 (P25, Degussa AG, Germany) was modified through hydrothermal and sol-gel methods (see Section 2.2 and 2.3), producing various catalysts. This study explores the modification of TiO_2 using advanced synthesis techniques to improve photocatalytic efficiency for antibiotic degradation, addressing current challenges such as low efficiency and long reaction times under practical conditions.

Deionized water and additional chemicals, including NaOH and H_2SO_4 (Xilong, China), were used for pH modification. For the free radical trapping test, tert-butyl alcohol (TBA, Merck, Germany), p-benzoquinone (p-BQ, Tianjin Dengfeng, China), and sodium azide (NaN_3, HiMedia, India) were used.

To comprehensively evaluate the physical properties of the synthesized TiO_2-based materials, advanced analytical techniques were employed. Surface morphology and elemental composition were investigated using Scanning Electron Microscopy (SEM) coupled with Energy-Dispersive X-ray Spectroscopy (EDS) (Oxford Instruments, UK). The SEM analysis was conducted at a magnification of 3500–5000×, with an accelerating voltage of 20 kV. The crystalline structure and phase composition were analyzed using X-ray Diffraction (XRD) (Bruker D8, Germany), with patterns compared against standard references (anatase PDF #00-021-1272, rutile PDF #00-021-1276) to confirm the crystallinity and phase purity. The XRD analysis was performed in a 2θ range of 10° to 80° with an increment of 0.0204° per step, and the X-ray wavelength was 1.5418 Å (Cu Kα). Additionally, the specific surface area and pore size distribution values were determined through Brunauer-Emmett-Teller (BET) analysis using nitrogen (N_2) as the adsorptive gas with a Micromeritics Gemini VII 2390t instrument (USA).

Control experiments were conducted during both characterization and photocatalytic activity testing. For SEM and EDS analysis, a P25 sample was analysed as a benchmark to confirm the accuracy of the imaging and elemental mapping results. Similarly, XRD and BET analyses included reference materials to ensure the reliable determination of crystalline structures, surface areas, and pore characteristics. In the photocatalytic activity tests, dark control experiments were carried out in the absence of light to evaluate the role of adsorption and to confirm that light-induced photocatalysis was the primary degradation mechanism responsible for the observed effects [24]. Finally, standard catalyst control experiments were performed using commercial TiO_2 (P25) as a benchmark to compare the performance of the synthesized materials.

Synthesis of TiO_2 Nanomaterial by a Hydrothermal Method

Catalysts were synthesized by a hydrothermal method [25]. The TiO_2/ZnO (TZ) catalyst was prepared by dissolving 0.17 g TiF_4, 1 g NaF, and 0.45 g $CO(NH_2)_2$ in 40 ml ethanol (solution A), and dissolving 0.6 g $Zn(Ac)_2.2H_2O$ and 0.3 g $C_6H_{12}N_4$ in 45 ml distilled water (solution B). Solutions A and B were mixed and stirred for 1 hour to produce solution C, which was transferred to a Teflon-lined autoclave, and heated at 160 °C for 24 hours. The product was centrifuged, washed with distilled water and ethanol, dried at 60 °C overnight, and calcined at 500 °C to get TZ-500 °C. The hydrothermal method was selected specifically for this synthesis due to its ability to produce highly crystalline materials with controlled morphology and particle size, which are essential for achieving enhanced photocatalytic performance.

To enhance the photocatalytic performance of the TiO_2/ZnO catalyst, reduced graphene oxide (rGO) was incorporated as a co-modifier. rGO is widely recognized for its excellent electrical conductivity and high surface area, which facilitate effective charge transfer and suppress electron-hole recombination, key factors for improving photocatalytic efficiency. The incorporation of rGO also enhances light absorption and provides additional active sites, promoting faster degradation of antibiotics. This modification is critical for addressing the limitations of pure TiO_2-based materials in practical applications.

Modified materials (TiO_2/ZnO/rGO 1%, 3%, 5%, namely TZR1, TZR3, TZR5) were prepared by adding rGO in varying ratios (1%, 3%, 5%) to the hydrothermal mixture. The rGO was dispersed in solution C before the hydrothermal process by ultrasonication for 30 minutes to ensure homogeneous distribution and prevent the aggregation of graphene oxide sheets. Specifically, 0.01 g, 0.03 g, and 0.05 g of rGO were added to prepare TZR1, TZR3, and TZR5, respectively. After the addition of rGO, the hydrothermal process and subsequent steps, including washing, drying, and calcination, followed the same procedure as for the unmodified TZ-500 °C catalyst. The use of rGO as a modifier in the synthesis process was intended to enhance the photocatalytic performance by improving charge transfer and electron-hole separation, thus promoting faster antibiotic degradation. The procedure was similar for the Pt-TZ and Ag-TZ catalysts. For Pt doping, an appropriate volume of H_2PtCl_6 aqueous solution was added to the mixture to achieve a nominal Pt loading of 0.5 wt%. For Ag doping, $AgNO_3$ was used as the precursor, and the process followed the same steps as the undoped TZ catalyst.

Synthesis of TiO_2-based Material by a Sol-gel Method

The base material, CS-TiO_2, was synthesized by dissolving 15 ml titanium isopropoxide (TiP) in 50 ml isopropanol and stirring for 1 hour, then mixing with 2 ml of 5 wt% chitosan in 100 ml acetic acid. After 3 hours of stirring, distilled water was added dropwise to form a suspension, which was centrifuged, washed, dried at 100 °C overnight, and then calcined at 500 °C for 3 hours.

The doped CS-TiO_2 were synthesized via a sol-gel method with precious metal doping [26]. These metals were chosen due to their distinct roles in improving the photocatalytic activity of TiO_2. Ag is known to increase visible-light absorption and facilitate charge separation by forming Schottky junctions with TiO_2 [27]. Pt acts as an electron sink, reducing recombination rates of photogenerated electron-hole pairs, while Pd enhances photocatalytic performance by acting as an electron trap and promoting the formation of reactive oxygen species [28].

Pd-doped TiO_2 catalysts (PdTi) were prepared by adding $Pd(NO_3)_2$ to the TiP solution before mixing with chitosan and proceeding as above. PdTi (0.75) and PdTi (0.5) were prepared similarly by adjusting $Pd(NO_3)_2$ to 0.75 % and 0.5 % (wt), respectively [29]. These dopants were incorporated to enhance the photocatalytic degradation of organic pollutants, including antibiotics, by improving light utilization and catalytic efficiency. The synthesis details for the TiO_2-based catalysts, including the doping of precious metals (Ag, Pt, Pd), are summarized in **Table 1**, which provides an overview of the catalyst compositions and preparation methods used in this study.

Experimental Design

This study assessed the photocatalytic treatment efficiency of various materials, including commercial P25 and synthesized variants, using LEVO degradation as the indicator over durations of 30 to 300 minutes. The photochemical process was initiated at various intervals of 0, 5, 10, 15, 20, 25, 30, 45, 60, 90, 120, 180, 210, 240, 270, and 300 minutes. Materials with superior treatment efficiency within shorter timeframes were further analysed.

LEVO degradation was investigated under varying conditions such as different pollutant-catalyst ratios and pH variations (3-10). TiO_2 photocatalyst materials were tested with LEVO at a concentration of 10 mg/L and a LEVO to photocatalyst ratio of 1:20 [30; 31]. The duration of a 30-minute pre-treatment was carried out to ensure that LEVO adsorption onto the catalyst surface reached equilibrium, thereby isolating the photocatalytic degradation process during the subsequent UV irradiation phase before starting the photochemical process (dark control experiment with adsorption sample (ADS) phase). The LEVO removal efficiency was calculated using Equation 1:

$$LEVO\ removal\ efficiency = \frac{C_0 - C_t}{C_0} \times 100\% \qquad (1)$$

Where C_0 (mg/L) represents the initial LEVO concentration and C_t (mg/L) is the LEVO concentration at time t.

Table 1. Summary of synthesized TiO_2-based catalysts with their compositions and preparation methods.

No.	Sample ID	Composition	Preparation Method	Key features/Modifications
1	TZ-500 °C	TiO_2/ZnO	Hydrothermal method	TiF_4, NaF, $CO(NH_2)_2$ in ethanol (Solution A); $Zn(Ac)_2 \cdot 2H_2O$, $C_6H_{12}N_4$ in water (Solution B); calcined at 500 °C.
2	TZR1	TiO_2/ZnO with 1 % reduced graphene oxide (rGO)	Hydrothermal method	Prepared by adding 1 % rGO to the hydrothermal mixture.
3	TZR3	TiO_2/ZnO with 3 % reduced graphene oxide (rGO)	Hydrothermal method	Prepared by adding 3 % rGO to the hydrothermal mixture.
4	TZR5	TiO_2/ZnO with 5 % reduced graphene oxide (rGO)	Hydrothermal method	Prepared by adding 5 % rGO to the hydrothermal mixture.
5	CS-TiO_2	TiO_2 doped with precious metals (Ag, Pt, Pd)	Sol-gel method	TiP in isopropanol mixed with chitosan in acetic acid; calcined at 500 °C.
6	PdTi (0.75)	TiO_2 doped with 0.75 % Pd	Sol-gel method	$Pd(NO_3)_2$ added to TiP solution before mixing with chitosan; calcined at 500 °C.
7	PdTi (0.5)	TiO_2 doped with 0.5 % Pd	Sol-gel method	$Pd(NO_3)_2$ added to TiP solution before mixing with chitosan; calcined at 500 °C.
8	PtTZ	TiO_2/ZnO doped with Pt	Sol-gel method (adapted for Pt doping)	Prepared by adding H_2PtCl_6 aqueous solution to the hydrothermal mixture to achieve a nominal Pt loading of 0.5 wt%.
9	AgTZ	TiO_2/ZnO doped with Ag	Sol-gel method (adapted for Ag doping)	$AgNO_3$ is used as the precursor, and the process follows the same steps as the undoped TZ catalyst

Photocatalytic experiments used natural light, UV LEDs, and a UVA lamp [30; 31; 32]. The UV LED source comprised 150 diodes (24V, 365 nm), ensuring uniform light exposure. The UVA lamp (8W, 365 nm) was positioned above the reactor for consistent photon flux. Natural light experiments utilized ambient sunlight. All trials were conducted in a controlled reactor for 150 minutes, with light intensity measured by a photometer to compare degradation efficiency under identical conditions.

Response Surface Methodology (RSM) optimized LEVO degradation with photocatalytic materials, examining four factors: pH (X_1, 3-9), antibiotics-to-materials ratio (X_2, 1:1 to 1:50), light intensity (X_3), and LEVO removal efficiency (Y) [33]. A central composite design (CCD) was used [34], and data were fitted to a second-order polynomial model (Equation 2) [35]:

$$Y = \beta_0 + \beta_1 X_1 + \beta_2 X_2 + \beta_3 X_3 + \beta_4 X_1^2 + \beta_5 X_2^2 + \beta_6 X_3^2 + \beta_7 X_1 X_2 + \beta_8 X_1 X_3 + \beta_9 X_2 X_3 \quad (2)$$

where Y is the response, X_1, X_2, and X_3 represent the independent variables, and β represents the regression coefficients that quantify the relationship between the independent variables (pH, antibiotics-to-materials ratio, and light intensity) and the response variable (LEVO removal efficiency).

Mathematical modelling (first-order linear (Equation 3), and the Langmuir-Hinshelwood equation (Equation 4)) provided insights into treatment efficiency [36]:

$$\ln\left(\frac{Co}{Ct}\right) = k_{obs} \times t \quad (3)$$

$$\frac{1}{k_{obs}} = \frac{1}{K_c} \times K_{L-H} + \frac{C_o}{K_c} \quad (4)$$

Here, k_{obs} represents the observed rate constant of LEVO decomposition (min^{-1}), C_0 denotes the initial concentration of LEVO ($mg.L^{-1}$), and C_t is the concentration of LEVO at time t ($mg.L^{-1}$). K_C represents the surface reaction rate ($mg.L^{-1}.min^{-1}$), and K_{L-H} represents the adsorption equilibrium constant ($L.mg^{-1}$) [37]. This experimental setup and mathematical model provide a comprehensive analysis of photocatalytic treatment efficiency under varied conditions, allowing for the identification of the most effective catalysts and conditions for the removal of antibiotics in wastewater.

RESULTS AND DISCUSSION

Material Selection for Subsequent Experiments and Discussion

The treatment efficiency of most materials reached a saturation point after 180 minutes, as shown in **Table 1** and **Figure 1**. Among the synthesized materials, PtTZ demonstrated the highest removal efficiency, achieving approximately 73 %, while P25 and CS-TiO_2 materials exhibited superior performance within the 180-minute timeframe, with removal efficiencies of 71.3 % and 69.36 %, respectively (as depicted in **Figure 1)**. This highlights the superior photocatalytic properties of these materials compared to others.

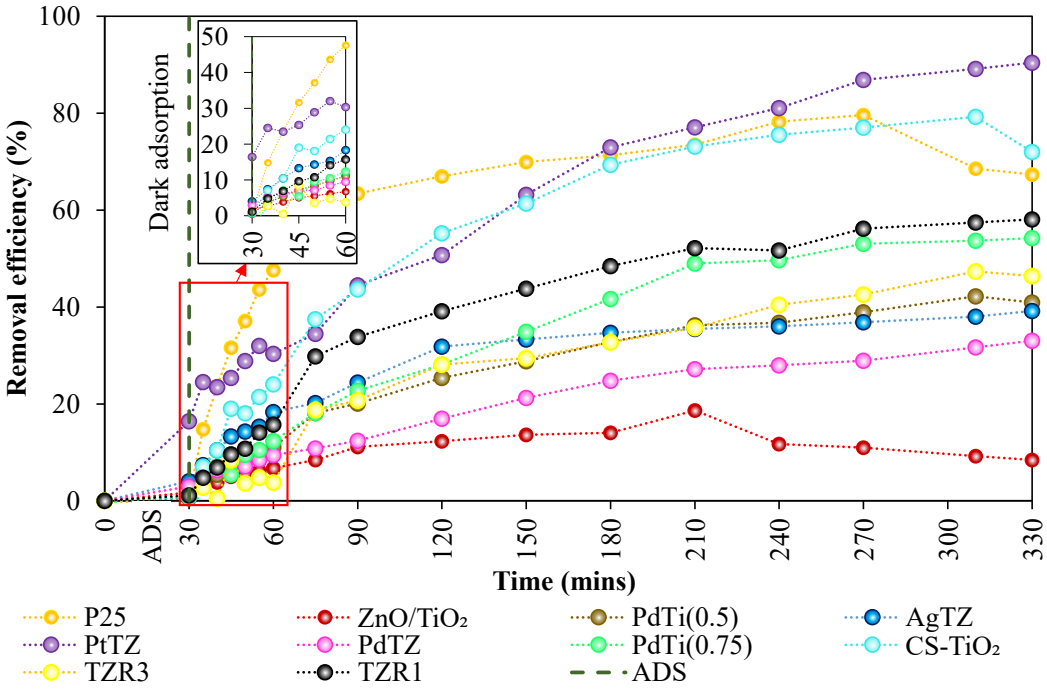

Figure 1. Removal efficiency of LEVO for catalysts synthesized via sol-gel and hydrothermal methods over time.

Synthesized materials were generally less efficient than commercial P25, with sol-gel synthesized materials outperforming hydrothermally synthesized ones. The superior performance of sol-gel-derived materials can be attributed to their smaller particle sizes, higher surface area, and enhanced porosity, which contribute to better light absorption, greater availability of active sites, and overall improved photocatalytic activity. For example, PtTZ and PdTi(0.75), synthesized via the sol-gel method, achieved removal efficiencies of 89.13 % and 53.7 %, respectively, after 280 minutes of UV radiation, whereas TZR1 and TZR3, prepared via the hydrothermal method, achieved only 57.44 % and 47.35 % under similar conditions.

The higher mass percentage of rGO in hydrothermal samples (e.g. TZR3) likely contributed to improved adsorption properties, enhancing the initial uptake of LEVO before photocatalytic reaction. For example, TZR3 exhibited partial removal of LEVO during the adsorption phase (2.79 %), outperforming many other catalysts in this regard. However, its overall photocatalytic efficiency remained lower than that of sol-gel-synthesized materials, suggesting that while adsorption was beneficial, photocatalytic activity remained the primary determinant of performance. Importantly, the inherent adsorption properties of the TiO_2 catalysts played a significant role in overall removal efficiency. While most materials demonstrated some degree of LEVO adsorption, TZR3 and PdTi(0.75) exhibited partial removal of LEVO even before the photochemical reaction began, indicating their superior adsorption capacity. This suggests that adsorption played a role in the overall removal efficiency, likely enhancing the subsequent photocatalytic degradation process.

Among the tested materials, P25 showed the highest removal efficiency, exceeding 70 % after 120 minutes of irradiation. This superior performance is attributed to its well-established photocatalytic properties, higher surface area for adsorption, and potentially favourable surface charges influencing adsorption and degradation. Based on these findings, P25 and CS-TiO_2 were selected for further experimentation, as their combined adsorption and photocatalytic properties demonstrated consistent and superior LEVO treatment outcomes.

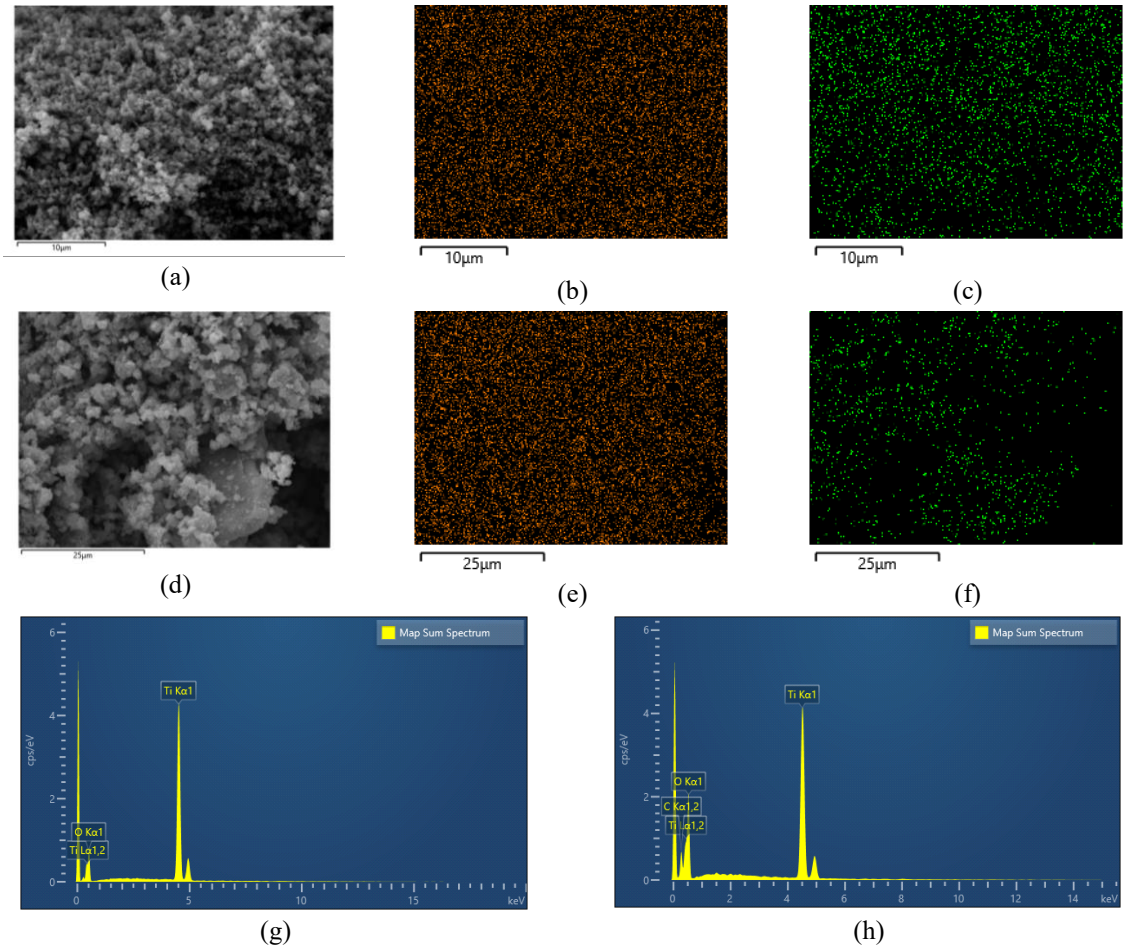

Figure 2. Comparative analysis of pristine P25 and CS-TiO_2: (a) electron image of pristine P25, (b) Ti Kα1 map of pristine P25, (c) O Kα1 map of pristine P25, (d) electron image of CS-TiO_2, (e) Ti Kα1 map of CS-TiO_2, (f) O Kα1 map of CS-TiO_2, (g) EDS spectrum of pristine P25, (h) EDS spectrum of CS-TiO_2.

Properties of Selected TiO_2-based Catalysts

The SEM images revealed an agglomeration of irregularly-shaped TiO_2 particles (**Figure 2**(a)). The high surface area of the powder was evident by the presence of numerous interparticle voids throughout the image. The absence of features corresponding to other polymorphs like rutile or brookite indicated a high degree of phase purity.

In **Figure 2(g)**, EDS analysis of the P25 sample revealed a predominance of titanium (Ti) and oxygen (O), with Ti showing the highest peak intensity at around 4.5 keV and O appearing around 0.5 keV, consistent with the composition of TiO_2. The carbon (C) peak at 0.3 keV indicated a lower concentration, likely due to surface contamination or minor impurities. The minor presence of C was negligible, reinforcing the sample's high purity. The results of SEM and EDS mapping revealed that P25 consisted of uniformly granular, nano-sized particles that were well-dispersed in water. In comparison, the electron image of CS-TiO_2 showed a close-up of a pile of irregularly shaped particles (**Figure 2(d)**). The particles appeared to be agglomerated, some parts in the shape of a bulk triangle covered with differently-shaped smaller particles. The magnification (3,500x) and image width (25 µm) suggest the particles were likely on the order of a few microns in size. EDS analysis (**Figure 2(h)**) did not detect the presence of any impurities, confirming the high purity of the TiO_2 sample.

Employing a Bruker diffractometer with Cu-Kα X-rays (λ=1.5418Å), XRD analysis meticulously scanned a 2θ range of 10° to 80° with precise step increments of 0.02° (depicted in **Figure 3**). Our investigation focused on unravelling the crystalline composition of both the P25 nanoparticles and our synthesized sample, CS-TiO_2. Comparisons between the XRD patterns of CS-TiO_2 and the industry standard, P25 yielded compelling insights (see **Figure 3)**. Noteworthy diffraction peaks at 2θ values of 25.4°, 48.1°, and additional peaks at 37.8°, 54.6°, and 62.1°, corresponded to crystal planes (011), (020), (004), (121), and (123), respectively, confirming the anatase structure of TiO_2. Intriguingly, while pristine P25 showcased the exclusive presence of the anatase phase, verified by crystallographic card number 96-900-8215, CS-TiO_2 exhibited subtle changes post-calcination, resulting in minor reductions in peak intensity.

The BET analysis of samples P25 and CS-TiO_2 is shown in **Figure 4**. The surface area analysis of P25 revealed a notable BET surface area of 114.17 m^2/g, indicating abundant active sites for interactions, alongside discernible meso- and macropores with significant cumulative volumes. This value was in line with expectations for anatase TiO_2 nanoparticles, which typically exhibit surface areas in the range of 50-200 m^2/g [38]. This high surface area provides a larger number of active sites. This is often associated with enhanced photocatalytic performance, as more reactants can adsorb onto the surface, facilitating their interaction with photo-generated charge carriers. The average pore width of approximately 70 Å suggests a mesoporous structure conducive to various applications, including effective photocatalysis.

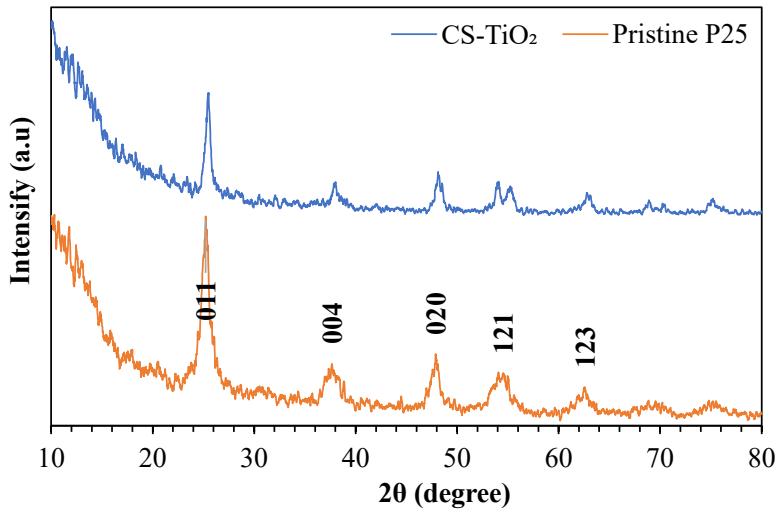

Figure 3. XRD analysis of pristine P25 (red line) and CS-TiO_2 (blue line).

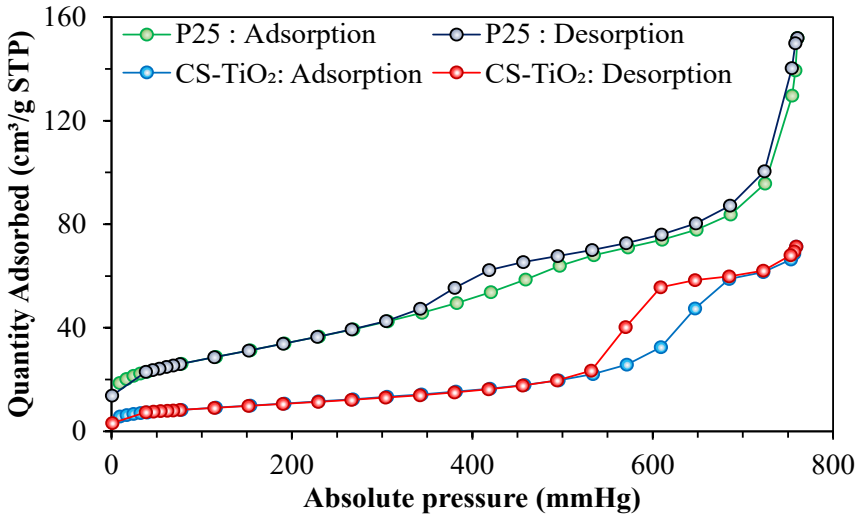

Figure 4. N_2 adsorption and desorption isotherms of P25 and CS-TiO_2.

In comparison, CS-TiO_2 revealed a surface area of 36.02 m^2/g, which was significantly lower than that of P25. Despite the lower surface area, CS-TiO_2 remained effective for pollutant degradation, likely due to its synthesis method and pore structure. The BJH analysis of the adsorption and desorption cumulative surface area of CS-TiO_2 revealed larger pores, with average pore widths of 103.52 Å (adsorption) and 90.98 Å (desorption). These larger pores may facilitate faster diffusion of reactants and more efficient surface reactions during photocatalysis. Therefore, despite the lower surface area, the mesoporous structure of CS-TiO_2, with its larger pore size, could enhance its photocatalytic activity in environmental applications such as pollutant degradation in water treatment.

Optimization of LEVO Treatment Conditions

Based on the scientific literature and experimental inquiries into LEVO processing, the treatment of LEVO antibiotic-containing synthetic wastewater employing CS-TiO_2 materials was observed to be subject to several influential variables, encompassing pH, reaction duration, antibiotic concentration in the water sample, catalyst material concentration, light intensity, and light energy. This investigation aimed to optimize the treatment of antibiotic-containing wastewater by investigating the impacts of four key factors: pH (X_1) within the range of 3 to 9, the Antibiotics to Materials ratio (X_2) ranging from 1:1 to 1:50, light intensity (X_3), and the antibiotic treatment efficiency (Y) serving as the objective function. Each experimental trial was meticulously executed for 150 minutes to procure a comprehensive dataset on the optimization process, as depicted in **Figure 5**.

During the experiment, pH was monitored continuously to evaluate its effect on LEVO degradation. The treatment efficiency reached a peak of 68.77 % at neutral pH (pH 7), attributed to an optimal balance between CS-TiO_2, surface charge, LEVO adsorption, and reactive species. At pH 7, the CS-TiO_2 surface charge was neutral, promoting better adsorption of neutral or slightly ionized LEVO molecules. Additionally, sufficient hydroxyl ions (HO^-) were available to support hydroxyl radical ($HO^\bullet$) formation, driving the degradation process. Deviation from pH 7, particularly in acidic or alkaline conditions, reduced hydroxyl radical formation and photocatalytic activity. Beyond pH 7, the efficiency dropped significantly, reaching 53.19 % at pH 8 and only 2.81 % at pH 9 (**Figure 5a**). Under acidic conditions (pH < 7), the positively charged TiO_2 surface promoted adsorption of negatively charged LEVO molecules via electrostatic attraction due to its point of zero charge (PZC), typically around pH 6-7 [39]. However, under highly acidic conditions (e.g., pH 3), limited HO^- availability resulted in reduced $HO^\bullet$ leading to lower efficiency (11.8 % after 150 minutes). Under alkaline conditions (pH > 7), the negatively charged CS-TiO_2 surface repelled deprotonated LEVO molecules, reducing adsorption efficiency. Excess HO^- ions in alkaline media promote the recombination of photogenerated electron-hole pairs, further decreasing $HO^\bullet$ and photocatalytic efficiency.

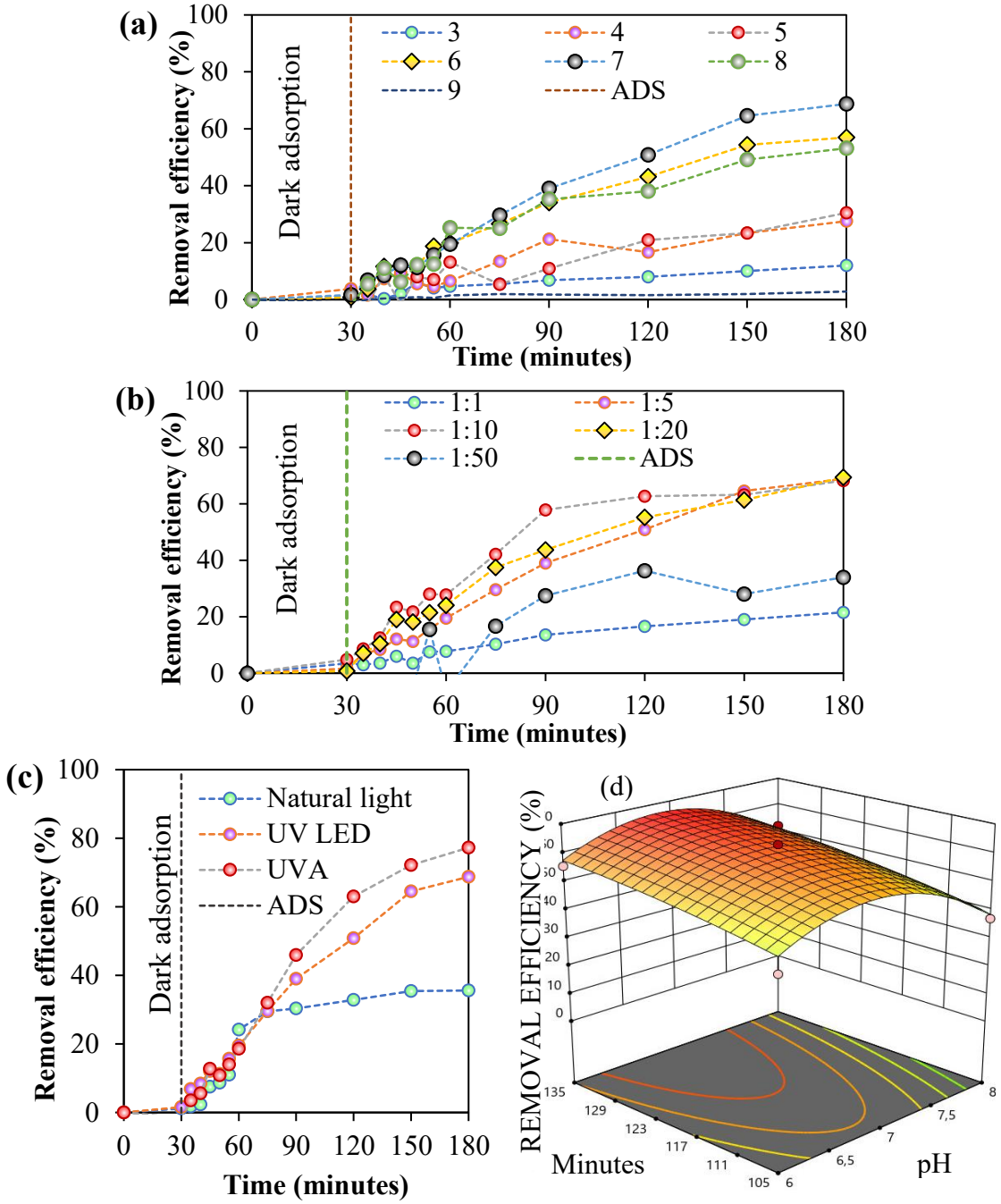

Figure 5. The effects of (a) pH level, (b) ratio of concentration of LEVO and material dosage, (c) types of light on LEVO degradation by catalyst CS-TiO_2, and (d) the 3D response surface.

Figure 5(b) shows that the LEVO degradation efficiency remained consistent at ratios of 1:5, 1:10, and 1:20, but decreased to 33.97 % at a 1:50 ratio. **Figure 5**(c) compares different light sources, showing that UVA lamp irradiation had the highest efficiency (77.29 %), followed by UV LEDs (68.77 %), and natural light (34 %). ANOVA tests indicated that pH significantly affected LEVO removal efficiency (p-value < 0.05). Reaction time also had a considerable effect (p-value < 0.05, quadratic relationship p = 0.0005). The 3D surface in **Figure 5**(d) illustrates the influence of pH (X_1) over time, showing a parabolic trend for pH and a linear influence of reaction time on LEVO removal efficiency (Y). The response surface showed that degradation efficiency peaked at a slightly acidic pH (6–7) due to generation of optimal reactive oxygen species (ROS) and TiO_2 activation. At neutral or basic pH, efficiency decreased. Reaction time had a linear effect, with efficiency increasing up to 135 minutes, after which it plateaued due to factors like LEVO depletion and electron-hole recombination. The quadratic pH-efficiency relationship underscores the importance of optimizing both pH and reaction time for effective LEVO treatment using CS-TiO_2.

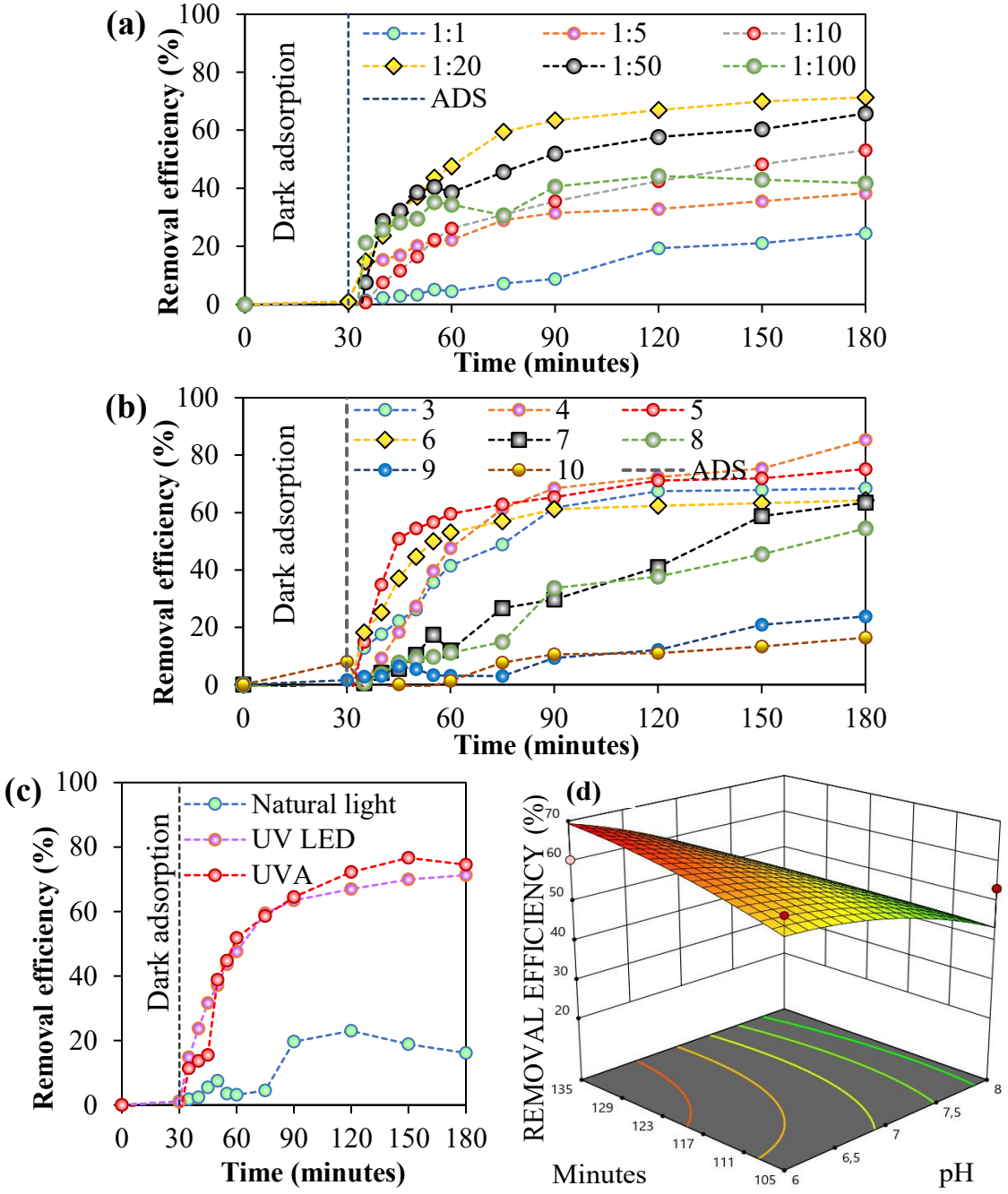

Figure 6. The effect of (a) pH level, (b) ratio of concentration of LEVO and material dosage, and (c) types of light on LEVO degradation by catalyst CS-TiO_2 (d) 3D response surface.

For P25 (commercial TiO_2), experiments explored the effects of pH, light conditions, and LEVO content on degradation efficiency over 150 minutes (**Figure 6**).

Figure 6(a) shows that in the pH range of 3 to 10, pH 4 yielded the highest efficiency (85.3 % at 150 minutes). **Figure 6**(b) indicates a 1:20 ratio achieved the highest efficiency (71.3 % at 180 minutes). **Figure 6**(c) demonstrates the superior performance of UVA lamps due to their higher intensity and better alignment with the TiO_2 light sources, showing higher efficiency under UVA lamp irradiation (74.53 %) compared to UVA LED (71.3 %) and natural light (16.13 %). The UVA lamp was approximately four times more efficient than UVA LED. Figure 6(d) shows a 3D response surface illustrating the interaction of pH and reaction time on LEVO degradation efficiency. Acidic conditions (pH 4–5) and extended reaction times (up to 150 minutes) yielded the highest photocatalytic efficiency, enhancing $HO^{\bullet}$ generation and surface interactions. The contour lines highlight the critical role of pH optimization, with longer reaction times promoting photon absorption and reactive species formation.

The choice of light sources significantly influenced LEVO degradation efficiency. Natural light, which contains a broad spectrum of wavelengths, exhibited the lowest efficiency (e.g., 16.13 % with P25 and 35.61 % with CS-TiO_2 at 150 minutes). This low performance may be attributed to the limited overlap between the visible light spectrum and the absorption properties of TiO_2, which primarily responds to UV wavelengths. UV LEDs, with a wavelength of 365 nm, offer more targeted activation of TiO_2 than natural light. However, their moderate intensity limits their performance compared to UVA lamps, as observed in the LEVO degradation efficiency of 68.77 and 71.3 % for CS-TiO_2 and P25, respectively, as their lower intensity generated fewer $HO^{\bullet}$ and superoxide ($O_2^{\bullet -}$) anions which are crucial for effective photodegradation. UVA lamps (365 nm) demonstrated the highest efficiency (e.g., 77.29 % with CS-TiO_2 and 74.53 % with P25 at 150 minutes) due to their stable wavelength output and consistent photon flux. This facilitated the excitation of TiO_2 electrons from the valence band to the conduction band, creating electron-hole pairs that drive the formation of ROS. The higher intensity also reduced electron-hole recombination, further enhancing the degradation process.

From Figures 5(c) and 6(c), CS-TiO_2 outperformed P25 under natural light, achieving 35.61 % efficiency compared to 16.13 %, likely due to its better adaptation to visible light wavelengths. With UV LEDs, both materials achieved similar degradation efficiencies (68.77 %), indicating comparable activation under moderate photon flux. Under UVA lamps, CS-TiO_2 showed a slightly higher efficiency (77.29 %) than P25 (74.53 %), highlighting its enhanced photocatalytic properties under high-intensity UV light. To further support these findings, an ANOVA test was conducted (**Table 2**), which showed significant differences in degradation efficiency based on the light source. The test indicated that the UVA lamp's stronger photon flux contributed to steeper increases in LEVO removal over time compared to UV LEDs and natural light. This reinforced the conclusion that light source selection is a critical factor in optimizing the photocatalytic degradation process. These trends emphasize the superior performance of CS-TiO_2 across all tested light sources, particularly under conditions of higher intensity and narrower wavelength alignment.

The ANOVA test (**Table 2**) revealed an R^2 value of 0.9862, indicating 98.62 % of data variation. The adjusted R^2 value of 0.9764 and the minimal difference between the adjusted R^2 and predicted R^2 coefficients (0.8723) confirmed the model's accuracy. The signal-to-noise ratio exceeded the threshold of 2, indicating strong predictive signal strength, while a coefficient of variation (C.V. %) of 5.98 % suggested precise experimental replication.

Table 2. ANOVA test for the model experiment of catalyst CS-TiO_2 and P25.

Data	CS-TiO_2	**P25**
Mean	49.45	53.20
C.V. %	5.98	12.59
R^2	0.9862	0.8469
Adjusted R^2	0.9764	0.7375
Predicted R^2	0.8723	-0.5569
Adeq Precision	32.3007	10.0979

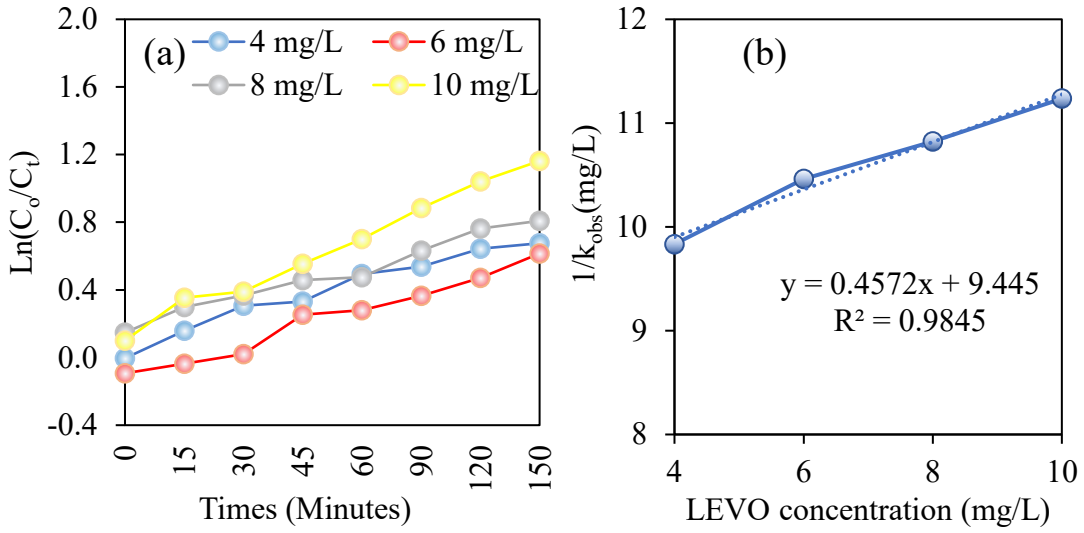

Figure 7. (a) Value of $\ln(C_o/C_t)$ against LEVO concentration in 150 min (b) reaction rate k_{obs} for LEVO degradation of catalyst CS-TiO_2.

For P25, only the pH level exhibited statistical significance ($p < 0.05$). The negative predicted R^2 suggests that the current model might not be an effective predictor of the response, implying that utilizing the mean of the data could be a more reliable approach. The reaction time represented the duration of contact between the photocatalyst material and the pollutant, with longer periods promoting greater photolysis. However, results indicated a p-value > 0.05, suggesting no significant difference in LEVO processing time within the chosen interval, indicating suboptimal performance. Therefore, further investigations with an extended time range are crucial to comprehensively explore the efficiency and impact of this photocatalyst on LEVO treatment.

Kinetics and Mechanisms of LEVO Photocatalysis

The relationship between the influent concentration and the efficiency of pollution treatment can be described by a first-order linear equation. Heterogeneous photocatalysis is often characterized by the Langmuir-Hinshelwood (L-H) equation. According to the L-H model, the rate of LEVO decomposition during photocatalysis is determined by the fraction of the surface occupied, as described by the Langmuir adsorption isotherm. The obtained linear equations exhibited high correlation coefficients (R^2 above 0.8) within the investigated concentration ranges, indicating the practical applicability and reliability of these equations (see Figure 7). Furthermore, the regression equation demonstrated a correlation coefficient of 0.9845, surpassing the confidence level of 0.5. Thus, it can be concluded that the reaction kinetics of LEVO followed the Langmuir-Hinshelwood kinetic model. The calculated values for K_C and $K_{L\text{-}H}$ were 0.0002 mg.L.min^{-1} and 484.06 L.mg^{-1}, respectively.

The photocatalytic reaction of LEVO utilizing TiO_2-based photocatalysts engenders active oxidizing species like $^1O_2$, $O_2^{\bullet-}$, photogenerated holes h^+, and $^{\bullet}OH$. Upon exposure to light of an appropriate excitation wavelength, electron-hole pairs are formed and conveyed to the material's surface, important in the generation of reactive oxygen species. To explore the influence of free radical formation on LEVO degradation, experiments were conducted using organic solvents such as tert-butyl alcohol (TBA), sodium azide (NaN_3), and p-benzoquinone (p-BQ) at a concentration of 1 mM to scavenge the free radicals. Notably, TBA demonstrated faster reactivity with $HO^{\bullet}$ compared to $SO_4^{\bullet-}$ ($k_{HO\bullet} = 3.8 - 7.6\times108$ m^{-1}.s^{-1}; $k_{SO4\bullet-} = 4 - 9.1\times105$ m^{-1}.s^{-1}), establishing it as the preferred scavenger for $^{\bullet}OH$ free radicals. Sodium azide was utilized to scavenge the $^1O_2$ radical and $HO^{\bullet}$, while p–BQ served to scavenge the $O_2^{\bullet-}$ superoxide radical [40]. Based on the optimized parameters mentioned earlier, the experimental conditions were set as follows: [LEVO] = 10 mg/L, [catalyst] = 50 mg/L, pH = 7, and a duration of 150 minutes, as depicted in **Figure 8**.

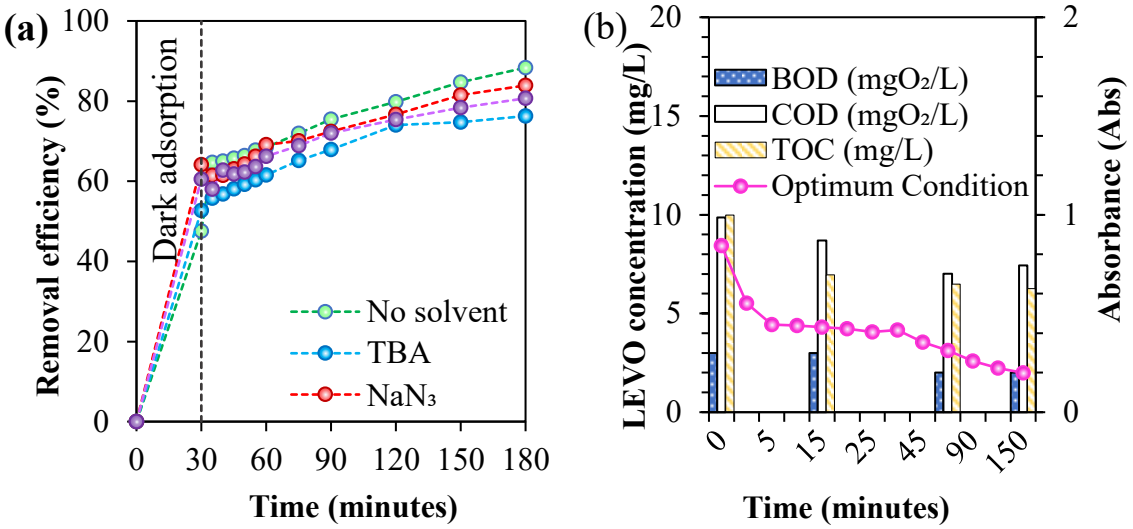

Figure 8. (a) LEVO degradation for various scavenger solvents, (b) Correlation of TOC, COD, and BOD reduction with LEVO removal by CS-TiO_2.

After a duration of 150 minutes, the removal efficiency of LEVO treatment using the CS-TiO_2 photocatalyst exhibited a decline from 88.33 % to 76.24 % when more than 10 % of free radical quenching solvents were introduced. Particularly, upon adding TBA, sodium azide (NaN_3), and p–benzoquinone (p–BQ) at equivalent concentrations, the sequence of treatment efficiency reduction manifested as follows: NaN_3 (83.91 %) > p–BQ (80.73 %) > TBA (76.24 %). These findings underscore the considerable role of generated free radicals in the efficiency of LEVO removal, with the hierarchical importance order being $^1O_2 > O_2^{\bullet-} > HO^{\bullet}$ (**Figure 8(a)**).

To augment the mineralization capacity of TiO_2-based photocatalysts in LEVO degradation, the research team conducted an evaluation of Total Organic Carbon (TOC) in the solution to assess carbon degradation. The outcomes demonstrated a reduction in TOC in comparison to the original wastewater sample, from 9.99 mg/L to 6.26 mg/L, as depicted in **Figure 8(b)**. Additionally, the Chemical Oxygen Demand (COD) exhibited a corresponding variation, decreasing from 9.86 mg O_2/L to 7.44 mg O_2/L. These observations indicate the photochemical degradation of LEVO by CS-TiO_2. The photocatalytic process of CS-TiO_2 potentially involves the subsequent reactions:

$$TiO_S + h\upsilon \rightarrow TiO_2\ (e^- + h^+)$$

$$O_2 + e^- \rightarrow O_2^{\bullet-}$$

$$O_2^{\bullet-} + H^+ \rightarrow HO_2^{\bullet}$$

$$2\ HO_2^{\bullet} \rightarrow O_2 + H_2O_2$$

$$H_2O_2 + e^- \rightarrow 2HO^{\bullet}$$

$$HO^{\bullet} + LEVO \rightarrow intermediates \rightarrow CO_2 + H_2O + F$$

The interactions between $HO^{\bullet}$ and organic pollutants play a key role in mineralizing organic pollutants. Radicals generated through these mechanisms engage in attacking and oxidizing organic pollutants, culminating in the photocatalytic degradation of organic substances [41]. P25 and CS-TiO_2 exhibited notable differences in photocatalytic efficiency and operating conditions compared to other catalysts in **Table 3**.

P25 demonstrated higher removal percentages (>85 %) than CS-TiO_2 (>70 %) under similar UV irradiation and duration conditions. However, both catalysts performed worse than Ag-deposited ZnO (99 %) and Ag-deposited TiO_2 (84 %), while Cu_2-xS/GCN NS and $MoS_2/Ag_2Mo_2O_7$ achieved 100 % and 97 % removal, respectively, under specific conditions. These comparisons highlight the importance of catalyst composition, light source, and operating parameters.

In summary, the TiO_2 materials synthesized by the sol-gel method in this study showed superior efficiency over hydrothermal composites. Optimal conditions for CS-TiO_2 and P25 involved specific pH levels, material ratios, and UV LED irradiation, and achieved over 70 % and 85 % efficiency, respectively. In comparison, CS-TiO_2 outperformed other TiO_2 catalysts at shorter reaction times. Advanced photocatalysts like Ag-deposited ZnO, $MoS_2/Ag_2Mo_2O_7$, and Cu_2-xS/GCN NS achieved higher removal efficiencies but required more energy or had scalability issues. Overall, CS-TiO_2 and P25 offer a practical balance of efficiency, cost-effectiveness, and scalability for wastewater treatment.

Table 3. Comparison of photocatalytic efficiency and operating conditions of various catalysts for LEVO removal.

Catalyst	Operating Conditions	Maximum Removal Percentage	References
0D/2D plasmonic Cu_2-xS/GCN NS	Xenon light, 25 °C, 20 min, Dose: 1 g/L	Complete removal (100 %)	[42]
TiO_2 nanoparticles	Visible light (40 W), 25 °C, 360 min, Dose: 0.5–2 g/L, Initial concentration: 25–100 mg/L, pH: 4, 7, 9	Nearly 83 % removal at 50 mg/L	[30]
GO-modified TiO_2 (3% carbon-doped)	LED visible light, 25 °C, 180 min, Dose: 1 g/L	74 % removal	[32]
Ag-deposited TiO_2	UV light, 25 °C, 150 min, Dose: 0.5–2 g/L, Initial concentration: 25 mg/L, pH: 6–7	Around 84 % (UV) and 49 % (visible) removal	[31]
$MoS_2/Ag_2Mo_2O_7$	Visible light (150 W), 25 °C, 90 min, Dose: 1 g/L	97 % removal	[43]
Ag-deposited ZnO	UV light (400 W) and visible light (500 W), 25 °C, 30 min adsorption in dark, Dose: 1 g/L, 5 wt% Ag/ZnO	Approximately 99 % (UV) and 56 % (visible) removal	[31]
CS-TiO_2	LED visible light, 25 °C, 150 min, Dose: 200 mg/L, LEVO: 10 mg/L, pH: 7	Approximately 70 % removal	This study
P25	LED visible light, 25 °C, 150 min, Dose: 200 mg/L, LEVO: 10 mg/L, pH: 4	Over 85 % removal	This study

CONCLUSION

TiO_2 photocatalyst materials synthesized via the sol-gel method, such as CS-TiO_2, PdTi, and P25, demonstrated enhanced LEVO treatment efficiency compared to hydrothermal composites like TZR, TZR1, TZR3, and AgTZ. Through experiments investigating factors influencing LEVO treatment efficiency, specific effective conditions for photocatalysts were established. For CS-TiO_2, a pH of 7, a LEVO:material ratio of 1:5, a duration of 150 minutes, and LED illumination resulted in an efficiency of approximately 70 %. Meanwhile, for P25, a pH of 4, a LEVO: material ratio of 1:20, a 150-minute duration, and LED lighting resulted in an efficiency surpassing 85 %. Notably, a 24V UV-LED strip with 150 diodes and an 8W UVA lamp featuring a light intensity of 6.5 W/cm^2 yielded similar efficiency when applied with CS-TiO_2. However, further research is warranted to elucidate the correlation between light intensity and antibiotic treatment efficiency, to delineate the optimal irradiation range for each antibiotic. This is crucial for the practical application of this treatment modality. The photocatalytic methodology was evaluated using first- and second-order kinetics equations, indicating the potential of TiO_2-based nanomaterials, particularly pure P25 and CS-TiO_2, in LEVO antibiotic treatment. While our study has provided valuable insights into the comparative

performance of P25 and CS-TiO_2 catalysts for LEVO degradation under controlled conditions, further research is needed to assess their performance in real wastewater samples, thus bridging the gap between laboratory findings and practical application.

ACKNOWLEDGEMENTS

This research was funded by Vietnam National University Ho Chi Minh City (VNU-HCM) under grant number: B2023-20-20. The authors acknowledge the time and facilities provided by Ho Chi Minh City University of Technology (HCMUT) and VNU-HCM, for this study.

REFERENCES

1. Zaman, S. B., Hussain, M. A., Nye, R., Mehta, V., Mamun, K. T. & Hossain, N. (2017) A Review on Antibiotic Resistance: Alarm Bells are Ringing. *Cureus*, **9(6)**, e1403.

2. Van Ngoc, T., Ngoc Thao, P. T. & Thanh Nga, T. T. (2017) Antimicrobial resistant characteristic of p. Aeruginosa and a. Baumannii caus. *Medical Journal*, 64–69.

3. Vinh Nghi, N., Van Hoi, T., Van Hong, N., Dong, N. & Thu Thao, N. T. (2017) Anti-infusal situation of normalalternatives at Ninh Thuan hospital in 2017 *Medical Journal, Topic Control of Bacteriophages*, 40–46.

4. Kümmerer, K., Dionysiou, D. D., Olsson, O. & Fatta-Kassinos, D. (2019) Reducing aquatic micropollutants–Increasing the focus on input prevention and integrated emission management. *Science of The Total Environment*, **652**, 836–850.

5. Yang, Q., Gao, Y., Ke, J., Show, P. L., Ge, Y., Liu, Y., Guo, R. & Chen, J. (2021) Antibiotics: An overview on the environmental occurrence, toxicity, degradation, and removal methods. *Bioengineered*, **12(1)**, 7376–7416.

6. Zhong, X., Zhang, K. -X., Wu, D., Ye, X. -Y., Huang, W. & Zhou, B. -X. (2020) Enhanced photocatalytic degradation of levofloxacin by Fe-doped BiOCl nanosheets under LED light irradiation. *Chemical Engineering Journal*, **383**, 123148.

7. Patel, M., Kumar, R., Kishor, K., Mlsna, T., Pittman Jr, C. U. & Mohan, D. (2019) Pharmaceuticals of emerging concern in aquatic systems: chemistry, occurrence, effects, and removal methods. *Chemical reviews*, **119(6)**, 3510–3673.

8. Gopal, G., Natarajan, C. & Mukherjee, A. (2022) Adsorptive removal of fluoroquinolone antibiotics using green synthesized and highly efficient Fe clay cellulose-acrylamide beads. *Environmental Technology & Innovation*, **28**, 102783.

9. Jatoi, A. S., Hashmi, Z., Adriyani, R., Yuniarto, A., Mazari, S. A., Akhter, F. & Mubarak, N. M. (2021) Recent trends and future challenges of pesticide removal techniques – A comprehensive review. *Journal of Environmental Chemical Engineering*, **9(4)**, 105571.

10. Scaria, J. & Nidheesh, P. V. (2022) Comparison of hydroxyl-radical-based advanced oxidation processes with sulfate radical-based advanced oxidation processes. *Current Opinion in Chemical Engineering*, **36**, 100830.

11. Liu, L., Chen, Z., Zhang, J., Shan, D., Wu, Y., Bai, L. & Wang, B. J. J. o. W. P. E. (2021) Treatment of industrial dye wastewater and pharmaceutical residue wastewater by advanced oxidation processes and its combination with nanocatalysts: A review, **42**, 102122.

12. Zhang, M. -H., Dong, H., Zhao, L., Wang, D. -X. & Meng, D. (2019) A review on Fenton process for organic wastewater treatment based on optimization perspective. *Science of The Total Environment*, **670**, 110–121.

13. Binh, V. N., Dang, N., Anh, N. T. K., Ky, L. X. & Thai, P. K. (2018) Antibiotics in the aquatic environment of Vietnam: Sources, concentrations, risk and control strategy. *Chemosphere*, **197**, 438–450.

14. Razzaq, Z., Khalid, A., Ahmad, P., Farooq, M., Khandaker, M. U., Sulieman, A., Rehman, I. U., Shakeel, S. & Khan, A. (2021) Photocatalytic and antibacterial potency of titanium dioxide nanoparticles: a cost-effective and environmentally friendly media for treatment of air and wastewater. *Catalysts*, **11(6)**, 709.

15. Bayan, E., Pustovaya, L. & Volkova, M. (2021) Recent advances in TiO2-based materials for photocatalytic degradation of antibiotics in aqueous systems. *Environmental Technology & Innovation,* **24**, 101822.

16. Gopinath, K. P., Madhav, N. V., Krishnan, A., Malolan, R. & Rangarajan, G. (2020) Present applications of titanium dioxide for the photocatalytic removal of pollutants from water: A review. *Journal of Environmental Management*, **270**, 110906.

17. Esposito, S. (2019) "Traditional" sol-gel chemistry as a powerful tool for the preparation of supported metal and metal oxide catalysts. *Materials*, **12(4)**, 668.

18. Mamaghani, A. H., Haghighat, F. & Lee, C. -S. (2019) Hydrothermal/solvothermal synthesis and treatment of TiO2 for photocatalytic degradation of air pollutants: Preparation, characterization, properties, and performance. *Chemosphere*, **219**, 804–825.

19. Sanakousar, F., Vidyasagar, C., Jiménez-Pérez, V. & Prakash, K. (2022) Recent progress on visible-light-driven metal and non-metal doped ZnO nanostructures for photocatalytic degradation of organic pollutants. *Materials Science in Semiconductor Processing,* **140**, 106390.

20. Mohamed, K., Benitto, J. J., Vijaya, J. J. & Bououdina, M. (2023) Recent advances in ZnO-based nanostructures for the photocatalytic degradation of hazardous, non-biodegradable medicines. *Crystals,* **13(2)**, 329.

21. Lu, K. -Q., Li, Y. -H., Tang, Z. -R. & Xu, Y. -J. (2021) Roles of graphene oxide in heterogeneous photocatalysis. *ACS materials Au*, **1(1)**, 37–54.

22. Mirikaram, N., Pérez-Molina, Á., Morales-Torres, S., Salemi, A., Maldonado-Hódar, F. J. & Pastrana-Martínez, L. M. (2021) Photocatalytic Perfomance of ZnO-Graphene Oxide Composites towards the Degradation of Vanillic Acid under Solar Radiation and Visible-LED. *Nanomaterials*, **11(6)**, 1576.

23. Ramesh, K., Gnanavel, B. & Shkir, M. (2021) Enhanced visible light photocatalytic degradation of bisphenol A (BPA) by reduced graphene oxide (RGO)–metal oxide (TiO2, ZnO and WO3) based nanocomposites. *Diamond and Related Materials*, **118**, 108514.

24. Rosa, D., Manetta, G. & Di Palma, L. (2024) Experimental assessment of the pH effect and ions on the photocatalytic activity of iron-doped titanium dioxide supported on polystyrene pellets: Batch and continuous tests. *Chemical Engineering Science*, **291**, 119918.

25. Masuda, Y. (2020) Ceramic nanostructures of SnO2, TiO2, and ZnO via aqueous crystal growth: cold crystallization and morphology control. *Journal of the Ceramic Society of Japan*, **128(10)**, 718–737.

26. Solanki, K., Parmar, D., Savaliya, C., Kumar, S. & Jethva, S. (2022) Surface morphology and optical properties of sol-gel synthesized TiO2 nanoparticles: Effect of Co, Pd and Ni-doping. *Materials Today: Proceedings*, **50**, 2576–2580.

27. Li, J., Jin, Z., Zhang, Y., Liu, D., Ma, A., Sun, Y., Li, X., Cai, Q. & Gui, J. (2022) Ag-induced anatase-rutile TiO2−x heterojunction facilitating the photogenerated carrier separation in visible-light irradiation. *Journal of Alloys and Compounds*, **909**, 164815.

28. Majeed, I., Ali, H., Idrees, A., Arif, A., Ashraf, W., Rasul, S., Khan, M. A., Nadeem, M. A. & Nadeem, M. A. (2022) Understanding the role of metal supported on TiO2 in photoreforming of oxygenates. *Energy Advances*, **1(11)**, 842–867.

29. Nguyen, C. H., Fu, C. -C. & Juang, R. -S. (2018) Degradation of methylene blue and methyl orange by palladium-doped TiO2 photocatalysis for water reuse: Efficiency and degradation pathways. *Journal of Cleaner Production*, **202**, 413–427.

30. Varma, K., Shukla, A., Tayade, R., Mishra, M., Nguyen, V. -H. & Gandhi, V. (2022) Interaction of levofloxacin with reverse micelle sol-gel synthesized TiO2 nanoparticles: Revealing ligand-to-metal charge transfer (LMCT) mechanism enhances photodegradation of antibiotics under visible light. *Materials Letters,* **309**, 131304.

31. Jandaghian, F., Ebrahimian Pirbazari, A., Tavakoli, O., Asasian-Kolur, N. & Sharifian, S. (2023) Comparison of the performance of Ag-deposited ZnO and TiO2 nanoparticles in levofloxacin degradation under UV/visible radiation. *Journal of Hazardous Materials Advances*, **9**, 100240.

32. Nair, N. G., Gandhi, V. G., Modi, K. & Shukla, A. (2024) Photocatalytic degradation of levofloxacin by GO-TiO2 under visible light. *Materials Today: Proceedings*.

33. Boutra, B., Sebti, A. & Trari, M. (2022) Response surface methodology and artificial neural network for optimization and modeling the photodegradation of organic pollutants in water. *International Journal of Environmental Science and Technology*, **19(11)**, 11263–11278.

34. Asman, S., Athirah Mohd Idris, A. & Pandian Sambasevam, K. (2024) Molecularly imprinted polymer based on deep eutectic solvent as functional monomer for paracetamol adsorption. *Journal of Molecular Liquids*, **408**, 125365.

35. Sateria, S. F., Norsham, I. N., Sambasevam, K. P. & Baharin, S. N. A. (2023) Photocatalytic Degradation of Perfluorooctanoic Acid (PFOA) using Molybdenum Disulphide-Graphene Oxide Composite via Box-Behnken Design Optimization. *Malaysian Journal of Chemistry*, **25 (3)**, 368–377.

36. Nasiri, A., Tamaddon, F., Mosslemin, M. H., Amiri Gharaghani, M. & Asadipour, A. (2019) Magnetic nano-biocomposite CuFe2O4@ methyl-cellulose (MC) prepared as a new nano-photocatalyst for degradation of ciprofloxacin

from aqueous solution. *Environmental Health Engineering and Management Journal*, **6(1)**, 41–51.

37. Malakootian, M., Nasiri, A. & Amiri Gharaghani, M. (2020) Photocatalytic degradation of ciprofloxacin antibiotic by TiO2 nanoparticles immobilized on a glass plate. *Chemical Engineering Communications*, **207(1)**, 56–72.

38. Žerjav, G., Žižek, K., Zavašnik, J. & Pintar, A. (2022) Brookite vs. rutile vs. anatase: What`s behind their various photocatalytic activities? *Journal of Environmental Chemical Engineering*, **10(3)**, 107722.

39. Zheng, F., Queirós, J. M., Martins, P. M., de Luis, R. F., Fidalgo-Marijuan, A., Vilas-Vilela, J. L., Lanceros-Méndez, S. & Reguera, J. (2023) Au-sensitised TiO2 and ZnO nanoparticles for broadband pharmaceuticals photocatalytic degradation in water remediation. *Colloids and Surfaces A: Physicochemical and Engineering Aspects*, **671**, 131594.

40. Gao, Z., Zhang, D. & Jun, Y. S. (2021) Does tert-butyl alcohol really terminate the oxidative activity of *OH in inorganic redox chemistry? *Environ. Sci. Technol.,* **55(15)**, 10442–10450.

41. Wen, X. -J., Niu, C. -G., Guo, H., Zhang, L., Liang, C. & Zeng, G. -M. (2018) Photocatalytic degradation of levofloxacin by ternary Ag2CO3/ CeO2/AgBr photocatalyst under visible-light irradiation: Degradation pathways, mineralization ability, and an accelerated interfacial charge transfer process study. *Journal of Catalysis*, **358**, 211–223.

42. Zhou, L., Liu, Z., Guan, Z., Tian, B., Wang, L., Zhou, Y., Zhou, Y., Lei, J., Zhang, J. & Liu, Y. (2020) 0D/2D plasmonic Cu2-xS/g-C3N4 nano-sheets harnessing UV-vis-NIR broad spectrum for photocatalytic degradation of antibiotic pollutant. *Applied Catalysis B: Environmental*, **263**, 118326.

43. Adhikari, S., Mandal, S. & Kim, D. -H. (2019) Z-scheme 2D/1D MoS2 nanosheet-decorated Ag2Mo2O7 microrods for efficient catalytic oxidation of levofloxacin. *Chemical Engineering Journal*, **373**, 31–43.